PHYSICAL REVIEW B **80**, 220502(R) (2009)

Direct dynamical coupling of spin modes and singlet Josephson supercurrent in ferromagnetic Josephson junctions

I. Petković,[1,*] M. Aprili,[1] S. E. Barnes,[2,3] F. Beuneu,[4] and S. Maekawa[5,6]

[1]*Laboratoire de Physique des Solides, UMR 8502, Bâtiment 510, Université Paris-Sud, 91405 Orsay Cedex, France*

[2]*Theory of Condensed Matter Group, Cavendish Laboratory, Madingley Road, Cambridge CB3 0HE, United Kingdom*

[3]*Physics Department, University of Miami, Coral Gables, Florida 33124, USA*

[4]*Laboratoire des Solides Irradiés, École Polytechnique, CNRS, F-91128 Palaiseau, France*

[5]*Institute for Materials Research, Tohoku University, Sendai 980-8577, Japan*

[6]*CREST, Japan Science and Technology Agency, Sanbancho, Tokyo 102-0075, Japan*

(Received 20 October 2009; published 3 December 2009)

Via a direct coupling between the order parameter and the singlet Josephson supercurrent we detect spin-wave resonances and their dispersion in ferromagnetic Josephson junctions in which the usual insulating or metallic barrier is replaced with a weak ferromagnet. The coupling arises within the Fraunhofer interferential description of the Josephson effect because the magnetic layer acts as a time-dependent phase plate. A spin-wave resonance at a frequency ω_s implies a dissipation that is reflected as a depression in the current-voltage curve of the Josephson junction when $\hbar\omega_s=2eV$. We have thereby performed a resonance experiment on only 10^7 Ni atoms.

DOI: 10.1103/PhysRevB.80.220502 PACS number(s): 74.50.+r, 74.45.+c, 85.25.Cp

The coupled dynamics of the electromagnetic field and a Josephson junction has a number of manifestations and is very well understood.[1–4] When the usual insulating or metallic barrier is replaced with a weak ferromagnet there is a coupling to another field, namely, the spontaneous magnetization of the ferromagnet. Spin waves are elementary spin excitations which can be viewed as both spatial- and time-dependent variations in the magnetization. In a ferromagnet the lowest-energy excitation, the ferromagnetic resonance (FMR), corresponds to the uniform precession of the magnetization around an external applied magnetic field at the frequency ω_s. This mode can be resonantly excited by an alternative (ac) magnetic field that couples directly to the magnetization as described by the Landau-Lifshitz equations.[5] The Josephson phase difference ϕ between the two superconductors has its own dynamics. A bias voltage V_0 causes ϕ to become time dependent so that $\phi=\phi_0+\omega_J t$, where $\omega_J=(2e/\hbar)V_0$ and ϕ_0 is arbitrary. The resulting ac Josephson current density is $J_s=J_c\sin(\phi_0+\omega_J t)$,[1] where J_c is the critical current density.

In analogy with the A-phase[6] of ^{3}He, coupled magnetic and phase oscillations should exist in ferromagnetic superconductors with triplet pairing, but have never been observed. We show here that a similar coupling for singlet superconductors can be realized in a Josephson junction with a ferromagnetic barrier. The dynamical coupling stems from the spatial interference of the Aharonov-Bohm phase caused by $\mathbf{M}(t)$, resulting in the spatial dependence of $\phi(\mathbf{r},t)$. The ac Josephson current produces an oscillating magnetic field $\mathbf{H}(t)$ and when the Josephson frequency matches the spin wave frequency, $\omega_J\approx\omega_s$, this resonantly excites $\mathbf{M}(t)$.[7] Due to the nonlinearity of the Josephson effect, there is a rectification of current across the junction, resulting in a dip in the average dc component of J_s at voltage $V_s=(\hbar/2e)\omega_s$. The principal result reported here is the observation of these coupled dynamics.

Magnetized Josephson junctions require weak ferromagnetic materials[8] and nanosized junction area to keep the overall magnetic flux in the junction smaller than the flux quantum Φ_0. We fabricated $Nb/Pd_{0.9}Ni_{0.1}/Nb$ Josephson junctions by *in situ* angle evaporation through a resist mask defined by *e*-lithography on a polyether sulphone (PES) (500 nm)/Si_3N_4(60 nm)/polymethyl methacrylate (PMMA) (350 nm) trilayer and etched in a reactive ion etching (RIE) chamber. The electron-gun evaporation is carried out in ultra-high-vacuum with a base pressure lower than 10^{-9} mbar. The PES is stable at temperatures reached during the evaporation of Nb. An electron microscope image of a typical ferromagnetic junction used in this Rapid Communication is shown in Fig. 1(a), while Fig. 1(b) is a schematic representation of the different layers. The superconducting electrodes comprise 50 nm of Nb (T_c=7.6 K), while the barrier is 20 nm of $Pd_{0.9}Ni_{0.1}$(T_{Curie}=150 K). The current-voltage (IV) characteristics are measured using current bias and are reported as function of the applied in-plane field, in the right insert of Fig. 2. The IV characteristics are not hysteretic, and overall they correspond closely to those expected for a junction with a conductive barrier.[9,10] The junction normal resistance is $R_n\approx 0.8\ \Omega$, and the Josephson coupling is $I_cR_n\approx 5.2\ \mu$V as expected for ferromagnetic junctions of this thickness,[8] yielding the critical supercurrent of $I_c\approx 6.7\ \mu$A. The hostile nature of even a weak ferromagnetic environment for singlet Cooper pairs is illustrated by a similar junction with 70 nm of non-magnetic Pd which, despite the almost four times larger thickness, has a larger critical current $I_c\approx 44\ \mu$A.

For a square junction of side L, the total supercurrent is given by the integral[11]

$$I_s = J_c\int_{-L/2}^{L/2} dx \int_{-L/2}^{L/2} dy\ \sin\phi(x,y,t), \qquad (1)$$

with

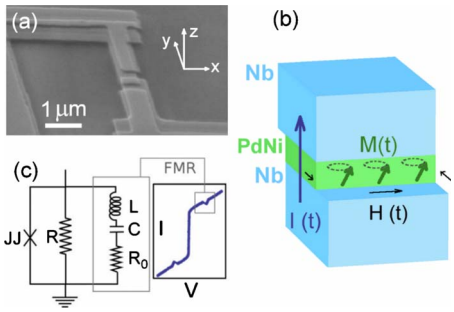

FIG. 1. (Color online) (a) SEM photo of the ferromagnetic Josephson junction used in the experiment. Junction area is 500×500 nm^2. (b) Schematic cross section of the Josephson junction. The ac Josephson current $I(t)$ flows through the junction creating an rf magnetic field $\mathbf{H}(t)$, causing the magnetization precession $\mathbf{M}(t)$, which in turn resonantly couples with the Josephson phase at frequency ω_J. Layers are, respectively, from the bottom: Nb (50 nm), $Pd_{0.9}Ni_{0.1}$ (20 nm), and Nb (50 nm). (c) The equivalent RSJ model and the sketch of the effect of the FMR on the current-voltage characteristics. The ferromagnetic layer is modeled as a series LCR oscillator, in parallel with the Josephson junction. Resistance R_0 is proportional to the imaginary part of the susceptibility χ''.

$$\phi(\mathbf{r},t) = \phi_0 + \omega_J t - \frac{2e}{\hbar}\int \mathbf{A}\cdot d\mathbf{r}, \tag{2}$$

where the last term is the Aharonov-Bohm phase,[12] involving the vector potential $\mathbf{A}$. We use a gauge where $\mathbf{A}=A(\mathbf{r},t)\hat{\mathbf{z}}$, the direction $\hat{\mathbf{z}}$ being perpendicular to the junction surface [see Fig. 1(a)]. Therefore $\phi(\mathbf{r},t)=\phi_0+kx+\omega_J t+\phi_m$, where $\phi_m=(4ae/\hbar)A_{mz}$ reflects time-dependent fields and

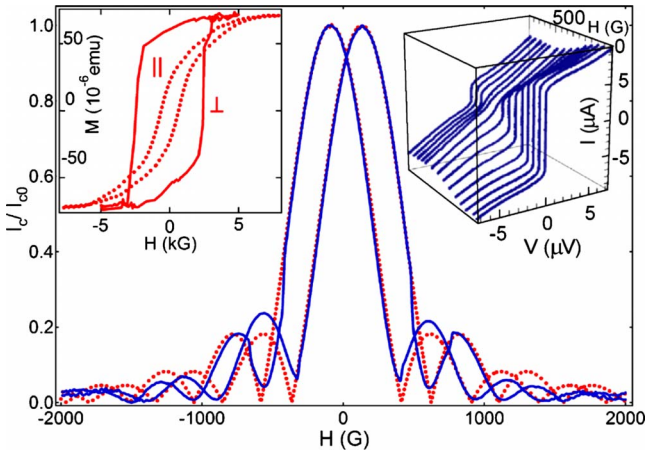

FIG. 2. (Color online) Dependence of the Josephson critical current on the external magnetic field in plane. The solid curve represents the normalized experimental data taken at 35 mK and the dotted curve is the Fraunhofer pattern expected for our junction parameters including the magnetization. Left insert: the magnetic hysteresis taken at 10 K on a millimetric trilayer with the same cross section as the junction, with field applied in plane (dotted curve) and perpendicular to the plane (solid curve). Right insert: current-voltage curves for different field values, measured at 35 mK.

$k=(4ed/\hbar)\mu_0 H+(4ea/\hbar)\mu_0 M_{0y}$. Here M_{0y} is the y component of the static magnetization $\mathbf{M_0}$, the applied field $\mathbf{H}$ is in the y direction, $2a$ and $2d=2(a+\lambda)$ are the actual and magnetic thickness of barrier and λ is the London penetration depth. Equations (1) and (2) are used to describe both the statics and the dynamics of our junctions.

When the time variable is disregarded, we are dealing with static fields, and Eqs. (1) and (2) lead to the Fraunhofer pattern $I_s=J_c L\int_{-L/2}^{L/2}dx\cos kx$[12] (we take $\phi_0=\pi/2$). The magnetization $\mathbf{M_0}$ of the barrier has the same effect as inserting a wedge-shaped phase plate in front of the slit, it displaces the diffraction pattern. Experimentally, the diffraction pattern is shifted to the right for increasing (positive M_{0y}) and the left for decreasing (negative M_{0y}) fields. This illustrates the linear nature of the coupling to $\mathbf{M}$. In Fig. 2, the dotted curves are a fit using Eqs. (1) and (2), along with the magnetization data measured on a trilayer with the same cross section as the junction (see the left insert of Fig. 2). The periodicity and the asymptotic behavior of the measured diffraction pattern attest to the high quality of our junctions. They confirm the close-to-uniform current distribution and single-harmonic current-phase relation, while the reproduction of the shift with the two sweep directions, using experimental magnetostatic data, confirms the validity of our description.

The dynamical coupling reflects a similar phase contribution $\varphi(\mathbf{r},t)$ due to $\mathbf{M}(\mathbf{r},t)$, but which now has both a temporal and a spatial dependence, the equivalent of a phase plate in the optical analog with a similarly dependent refractive index $n(\mathbf{r},t)$. The precession of the magnetization (time scale of 0.1–1 ns) is much slower than the diffusion time through the ferromagnetic layer (0.5 ps). The Josephson coupling is thus adiabatic with respect to the magnetization dynamics. This assumption is implicit in Eqs. (1) and (2). The nonadiabatic limit is considered in Ref. 13. The signal is seen for $V>I_cR$, implying Eq. (1) can be linearized. The dc magnetic signal then corresponds to[11]

$$I_m = \frac{4ae}{\hbar}\int_{-L/2}^{L/2}dx\int_{-L/2}^{L/2}dy J_c\,\overline{\cos(kx+\omega_J t)\phi_m}, \tag{3}$$

where the bar denotes a time average. Substituting for $\phi_m=(4ae/\hbar)A_{mz}$ and using $\mathbf{J}=\nabla\times\mathbf{H}$, following both a time and space integration by parts, the dc signal reflecting the magnetic resonance is

$$I_m = \frac{1}{V_0}\int d\mathbf{r}\overline{\mathbf{H}\cdot\frac{d\mathbf{M}}{dt}}, \tag{4}$$

with $M_i(\mathbf{r},t)=\int dt'\chi_i(t-t')H_i(\mathbf{r},t')$, $i=x,y,z$, where $\chi_i(t)$ is the dynamic susceptibility. This has an appealing interpretation in terms of magnetic losses. Here, as illustrated by Fig. 1(b), $\mathbf{H}(\mathbf{r},t)$ is the magnetic field which circulates inside the junction by virtue of the ac Josephson current. The junction lateral size L is smaller than both λ and the skin depth for the frequencies involved. The displacement current is therefore negligible and all that is needed is to integrate Ampere's law in order to determine $\mathbf{H}(\mathbf{r},t)$. More details of these calculations are given elsewhere.[14] The current due to $\mathbf{M}(\mathbf{r},t)$ is

$$I_m = \pi I_c(0)\frac{\Phi_{\rm rf}}{\Phi_0}[F_x\chi_x''(\omega_J) + F_y\chi_y''(\omega_J)], \quad (5)$$

where $\Phi_{\rm rf}=(2aL)B_{\rm rf}=(2aL)\mu_0 I_c(0)/L$ is the flux due to the radio-frequency field and $F_x=(1/48)[I_c(B_0)/I_c]^2$ and $F_y=(2/x^2)\{1-(1/x)\sin(x/2)\cos(x/2)-[(11/24)+(2/x^2)]\sin^2(x/2)\}$; $x=kL$, reflect the geometrical structure of the coupling. As the equilibrium magnetization is along the z axis, the magnetic resonance signal is contained in $\chi_x''(\omega_J)$ and $\chi_y''(\omega_J)$, the Fourier transforms of the imaginary part of the susceptibility. Therefore, the total dc current within the resistively shunted junction (RSJ) model[9,10] is

$$I = \frac{V_0}{R(0)} + \frac{I_c^2(B_0)}{2V_0}R(\omega_J) - I_m, \quad (6)$$

where $R(0)$ and $R(\omega_J)\approx R$ are the junction resistances for dc and frequency ω_J. A simple physical argument can account for the three terms in Eq. (6). The average power dissipated in the junction is IV_0 and so the first term, V_0^2/R, corresponds to the Ohmic loss at dc, while $\frac{1}{2}I_c^2R(\omega_J)$ is the similar loss at ω_J. The key third term represents a self-inductance $L(\mathbf{M})$, stemming from the ferromagnet, in parallel with the junction and modeled as an LCR oscillator [see Fig. 1(c)], where R_0 reflects the magnetic damping. At the magnetic resonance frequency, energy is absorbed by the ferromagnet, causing the oscillator to be lossy. This actually reduces the effective junction resistance, leading to a dip in $I(V)$. In this manner, the Josephson junction rectifies the self-induced magnetic resonance.

This coupling to the magnetic system is evident in the measured dynamical resistance dV/dI curves reported in Fig. 3. We measure the dynamical resistance rather than the IV characteristics to improve amplitude resolution. The mode labeled FMR is seen only for ferromagnetic junctions. There is good agreement between the experiment (solid curves) and theory (dotted curves). The magnetic resonance mode observed in our experiments reflects the properties of a thin film of the ferromagnet $Pd_{0.9}Ni_{0.1}$. Magnetization curves $M(H)$, measured directly for a large area Nb/PdNi/Nb trilayer with the same cross section as the junction, are shown in the insert of Fig. 2. They indicate that $\mathbf{M}$ is perpendicular to the junction plane, a conclusion reinforced by earlier anomalous Hall-effect measurements on similar thin films.[15] The FMR mode, shown in Fig. 3, occurs at $V_0=23\ \mu$V. This is unambiguously identified as such since the frequency $\omega_s=2eV_0/\hbar$ agrees, without fitting parameters, with the Kittel formula[16]

$$\omega_s = \gamma_e\sqrt{(H_K - 4\pi M_S)^2 - H^2} \quad (7)$$

for the in-plane magnetic field dependence of the uniform FMR mode when the anisotropy field is perpendicular to the plane. The anisotropy field $H_K=4900$ G and the magnetization at saturation $M_S=930$ G are both determined directly from the static magnetization data, and γ_e is the electron gyromagnetic ratio. For comparison, the ferromagnetic resonance of a macroscopic Nb/PdNi/Nb trilayer has been measured in a conventional 9.5 GHz cavity spectrometer at 10 K with field applied parallel to the substrate. The cavity FMR,

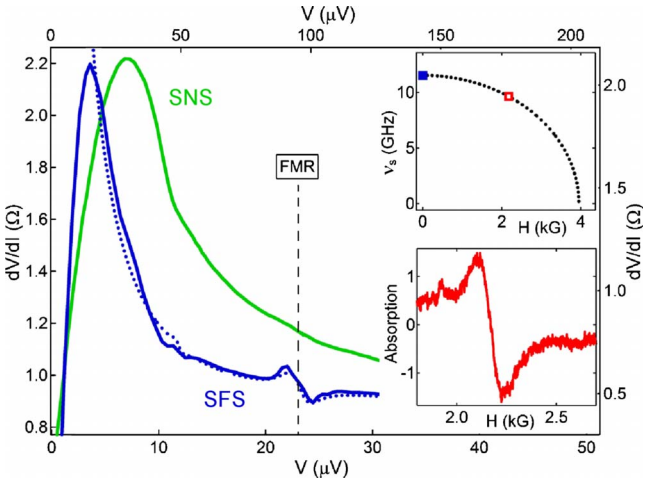

FIG. 3. (Color online) Dynamical resistance of the ferromagnetic Josephson junction (solid curve, SFS, bottom and left axis) shows resonances compared to a similar nonferromagnetic junction (solid curve, SNS, top and right axis). Dotted curve is a fit to theory [Eq. (6)]. The mode at 23 μV is the FMR. Bottom insert: conventional cavity ferromagnetic resonance on a macroscopic trilayer. Top insert: comparison between the field dependence of the FMR $\nu_s=\omega_s/2\pi$ in the Josephson junction (solid square) with the cavity measurement on a macroscopic trilayer (open square). Dotted curve is a parameter free fit of the FMR using the Kittel formula [Eq. (7)].

shown in the bottom insert of Fig. 3, occurs at 2160 G, again exactly as predicted by Eq. (7). Displayed in the top insert of Fig. 3 is the comparison of the resonant mode in the Josephson junction (solid square) and in the macroscopic trilayer (open square). The dotted curve shows the frequency of the FMR mode calculated from the Kittel formula [Eq. (7)]. The spectra presented in the main part of Fig. 3 contain an extrinsic broadening caused by a lock-in modulation voltage of $\sim 1\ \mu$V. For the ac modulation voltage of 0.5 μV, the junction resonance width saturates at 0.5 μV, which corresponds to the conventional resonance width (150 G). The signal amplitude corresponds to a resonant susceptibility of approximately 10, consistent with the FMR mode measured in a microwave cavity and reported in the bottom insert of Fig. 3.

In order to demonstrate that the magnetic system is coupled to the super but not to the normal current, we have performed Shapiro step[2] measurements, reported as the dynamical resistance dV/dI in Fig. 4(a). The junction is irradiated with microwaves of frequency $\nu=17.35$ GHz at 35 mK. The Shapiro steps arise from the mixing of the microwave signal with the ac Josephson effect and are smaller replicas of the zero-voltage current step displaced from zero voltage by $V_n=n(\hbar/2e)\omega$, where $\omega=2\pi\nu$ and n is an integer. We do not observe half-integer Shapiro steps, indicating negligible higher harmonics in the current-phase relation. However, as expected within the RSJ model, the ferromagnetic resonance can be excited at voltage $V_{ms}=(\hbar/2e)\omega_s/m$, m being an integer.[4] The subharmonic for $m=2$ is visible in the spectrum in Fig. 3. As shown in Fig. 4(a), it is reproduced as a sideband to each regular step when $V=(\hbar/2e)(n\omega\pm\omega_s/2)$. Experimentally, we do not have available a high enough frequency to separate similar sidebands for the main FMR mode at ω_s.

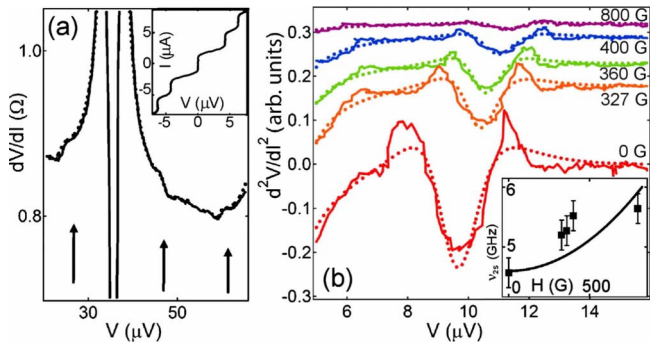

FIG. 4. (Color online) (a) The dynamical resistance of the ferromagnetic Josephson junction with applied external microwaves. Pronounced dip is the Shapiro resonance, and arrows indicate sideband resonances at the same frequency as the $m=2$ mode at 10 μV from Fig. 3. The external microwave frequency is 17.35 GHz and the temperature 35 mK. Insert: typical *IV* curve with applied external microwaves of 2 GHz at 35 mK, showing Shapiro steps. (b) Dependence of the $m=2$ FMR mode on the in plane magnetic field. Solid curves are the measured derivative of the dynamical resistance from Fig. 3, and dotted curves are a fit [Eq. (6)]. The spin-wave frequency increases with field. Insert: the field dispersion relation of the modes. The solid line is Eq. (7) when the spatial dependence of the FMR modes is taken into account.

Finally, the field dependence of the resonance at $\omega_s/2$ has been studied in more detail in the second derivative, d^2V/dI^2 [Fig. 4(b)], where the minima correspond to $V_{2s}=(\hbar/2e)\omega_s/2$. Measurements were limited in field due to the rapid decrease in the critical current above 800 G. In the insert of Fig. 4(b) we show $\nu_{2s}=(1/2\pi)\omega_s/2$ as a function of the applied magnetic field. The error bars are due to the drift of the amplifier. The solid line is Eq. (7), without fitting parameters, with the spatial dependence of FMR taken into account. The spatial dependence of the spin waves leads to an additional term to Eq. (7) given by ak^2, where $k=(\pi d/\Phi_0)H$ is the spin wave momentum and $a=E_{ex}b^2$, where $E_{ex}=50$ meV is the PdNi exchange energy and $b\approx 0.1$ nm the lattice constant. Since the width of the junction is only about 500 nm, this leads to a small but finite correction to the uniform FMR energy which is larger than the direct effect of the applied dc field. Illustrated in this manner is the direct determination of spin-wave dispersion using the present technique.

In conclusion, we have demonstrated the dynamical coupling of the superconducting phase with the spin waves in a ferromagnet and measured their dispersion. We have performed a photon free FMR experiment on about 10^7 Ni atoms, which would be infeasible with standard FMR techniques, and have illustrated a methodology for the study of spin dynamics. There are direct and implied applications to spintronics and nanomagnetism.[17]

We thank J. Gabelli, B. Reulet, D. Feinberg, R. Melin, Z. Radović, I. Martin, and M. Houzet for stimulating discussions; M.A. is indebted to H. Bouchiat for an illuminating conversation and to A. Thiaville and H. Hurdequint for many tutorials about spin dynamics. We acknowledge L. Ferlazzo of the LPN-Marcoussis for technical assistance with reactive ion etching. This work was in part supported by CREST of JST, and EPSRC-GB (U.K.).

*petkovic@lps.u-psud.fr

[1] B. D. Josephson, Phys. Lett. **1**, 251 (1962).
[2] S. Shapiro, Phys. Rev. Lett. **11**, 80 (1963).
[3] D. D. Coon and M. D. Fiske, Phys. Rev. **138**, A744 (1965).
[4] K. K. Likharev, *Dynamics of Josephson Junctions and Circuits* (Gordon and Breach, New York, 1986).
[5] C. Kittel, Phys. Rev. **115**, 1587 (1959).
[6] A. J. Leggett, Phys. Rev. Lett. **29**, 1227 (1972).
[7] K. Baberschke, K. D. Bures, and S. E. Barnes, Phys. Rev. Lett. **53**, 98 (1984); S. E. Barnes and F. Mehran, Phys. Rev. B **34**, 4537 (1986).
[8] T. Kontos, M. Aprili, J. Lesueur, F. Genet, B. Stephanidis, and R. Boursier, Phys. Rev. Lett. **89**, 137007 (2002).
[9] W. C. Stewart, Appl. Phys. Lett. **12**, 277 (1968).
[10] D. E. McCumber, J. Appl. Phys. **39**, 3113 (1968).
[11] A. Barone and G. Paterno, *Physics and Applications of the Josephson Effect* (Wiley, New York, 1982).
[12] P. W. Anderson and J. M. Rowell, Phys. Rev. Lett. **10**, 230 (1963).
[13] Z. Nussinov, A. Shnirman, D. P. Arovas, A. V. Balatsky, and J.-X. Zhu, Phys. Rev. B **71**, 214520 (2005); J.-X. Zhu, Z. Nussinov, A. Shnirman, and A. V. Balatsky, Phys. Rev. Lett. **92**, 107001 (2004).
[14] S. E. Barnes *et al.* (unpublished).
[15] T. Kontos, M. Aprili, J. Lesueur, and X. Grison, Phys. Rev. Lett. **86**, 304 (2001).
[16] C. Kittel, Rev. Mod. Phys. **21**, 541 (1949).
[17] *Concepts in Spin Electronics*, edited by S. Maekawa (Oxford University Press, New York, 2006).